Organic Electronics 39 (2016) 71–76

Contents lists available at ScienceDirect

Organic Electronics

journal homepage: www.elsevier.com/locate/orgel

All thermal-evaporated surface plasmon enhanced organic solar cells by Au nanoparticles

Yuan Gao [a, b], Fangming Jin [a], Zisheng Su [a, *], Haifeng Zhao [a], Yongshi Luo [a], Bei Chu [a, **], Wenlian Li [a]

[a] State Key Laboratory of Luminescence and Applications, Changchun Institute of Optics, Fine Mechanics, and Physics, Chinese Academy of Sciences, Changchun 130033, People's Republic of China
[b] University of Chinese Academy of Sciences, Beijing 100039, People's Republic of China

ARTICLE INFO

Article history:
Received 29 August 2016
Received in revised form
24 September 2016
Accepted 25 September 2016
Available online 30 September 2016

Keywords:
Organic solar cell
Small molecule
Localized surface plasmon resonance
Metal nanoparticle

ABSTRACT

Au nanoparticles (NPs) are fabricated on indium-tin-oxide substrates by a thermal evaporation method and incorporated to an efficient small molecule organic solar cell (OSC). This renders an all thermal evaporated surface plasmon enhanced OSC. The optimized device shows a power conversion efficiency of 3.40%, which is 14% higher than that of the reference device without Au NPs. The improvement is mainly contributed to the increased short-circuit current which resulted from the enhanced light harvesting due to localized surface plasmon resonance of Au NPs and the increased conductivity of the device.

© 2016 Elsevier B.V. All rights reserved.

1. Introduction

Organic solar cells (OSCs) have attracted much attention due to their potential of flexibility, low weight, and low-cost mass production. Though the power conversion efficiency (PCE) has improved gradually over the past few years, which is passed 10% [1–10], it is still significantly lower than that of inorganic counterparts and needs to be further improved for commercial applications. The PCE of an OSC is determined by the absorption efficiency, exciton dissociation efficiency, and charge carrier collection efficiency. The short exciton diffusion length and low carrier mobility of organic materials limit the thickness of organic active layer, resulting in the insufficient absorbance of OSCs [11–13]. Hence, an essential and simple method to improve the PCE is to increase the light absorption efficiency in the case of no influence on active layer thickness. However, increasing the light absorption of the active layer at a limited thickness remains to be a challenge, motivating the development of many kinds of light trapping techniques.

Localized surface plasmon resonance (LSPR) of metal nanoparticles (NPs) occurs when the incident photon frequency matches well with that of the metal NPs, and it could result in strong light scattering and local electromagnetic field enhancement. The LSPR effect can be controlled by adjusting the particle size, shape, spacing, dielectric properties, and dielectric environment, which are influential to the resonance absorption peak [14–17]. Recently, metal NPs have been incorporated into the OSCs to improve their absorption efficiency by triggering the LSPR [18–30]. The commonly used metal NPs are Ag and Au. Compared with Ag NPs, the higher permittivity of Au NPs leads to longer LSPR wavelength given that they have the same sharp and size, resulting in a better matching between the LSPR and the solar irradiation [31]. Au NPs can be fabricated by many methods, such as solution method [32–36], plasma assisted physical vapour deposition [23], and thermal evaporation [37–39]. Among these, thermal evaporation has attracted much attention due to its simple, fast, and cost-effective advantages for preparation of metal NPs. However, there are rare reported on thermal evaporated Au NPs for OSCs [37–39]. Xu et al. have demonstrated surface plasmon enhanced polymer solar cells by using thermal evaporated Au NPs [14]. In their devices, twice thermal evaporation processes are required as the organic active layers are processed with a solution method. From the cost point of view, the thermal evaporated Au NPs may be more

* Corresponding author.
** Corresponding author.
E-mail addresses: suzs@ciomp.ac.cn (Z. Su), chub@ciomp.ac.cn (B. Chu).

http://dx.doi.org/10.1016/j.orgel.2016.09.028
1566-1199/© 2016 Elsevier B.V. All rights reserved.

suitable for all thermal evaporated OSCs as all the layers can be thermal evaporated in sequence without a vacuum breaking.

In this work, we demonstrate an all thermal evaporated surface plasmon enhanced small molecule OSC by incorporating Au NPs to the 1,1-bis-(4-bis(4-methyl-phenyl)-amino-phenyl)-cyclohexane (DBP)/C_{70} based planar heterojunction device. MoO_3 anode buffer is combined in order to avoid exciton quenching by the Au NPs. As a result, the highest PCE of 3.40% was determined, which is increased by 14% as compared to the reference cell without Au NPs.

2. Experimental methods

The organic materials used for the OSCs were procured commercially and were used without further sublimation. Devices were fabricated on patterned ITO-coated glass substrates with a sheet resistance of 15 Ω/sq. Prior to deposition, the ITO substrates were cleaned in a series of solvents such as acetone, deionized water, and isopropyl alcohol, and then treated by ultraviolet-ozone in a chamber for 15 min. A series of devices with the structure of ITO/Au (x nm)/MoO_3/DBP (13 nm)/C_{70} (45 nm)/4,7-diphenyl-1,10-phenanthroline (Bphen) (8 nm)/Al (100 nm) were constructed, here x ranged from 0 to 1.0 nm, and the thickness of MoO_3 in each device was optimized to achieve the best performance. The device structure and molecular structures of DBP and C_{70} are illustrated in Fig. 1. All the layers, including Au, were deposited onto the substrates in sequence via thermal evaporation in the vacuum chamber at a pressure of 4×10^{-4} Pa without a vacuum breaking. Deposition rates were monitored with a quartz oscillating crystal and controlled to be 1 Å/s for Au, 0.5 Å/s for MoO_3 and the organic layers, and 5 Å/s for Al cathode. The area of the devices patterned by the shadow mask was 0.1 cm^2. Current density-voltage (J–V) characteristics of the devices were measured with a Keithley 2400 source meter under an AM 1.5G illumination (Newport 94023A) with a calibrated intensity of 100 mW/cm^2. The incident photon to current conversion efficiency (IPCE) spectra was performed with a Stanford SR803 lock-in amplifier under monochromatic illumination at a chopping frequency of 130 Hz by a Stanford SR540 chopper. Scanning electron microscopy (SEM) images were measured on a Hitachi S4800. Absorption spectra of the organic films on ITO-coated glass substrates were recorded with a Shimadzu UV-3101PC spectrophotometer. Steady-state photoluminescent (PL) spectra were measured with a Hitachi F7000 fluorescence spectrophotometer. Transient PL decay was measured with an Edinburgh FL 920 spectrometer at an excitation wavelength of 480 nm by using a hydrogen lamp. All the measurements were carried out at room temperature under ambient conditions.

3. Results and discussion

The thicknesses of Au layer and MoO_3 layer play important roles in determining the performance of the surface plasmon enhanced devices. For a thicker MoO_3 layer, the resistance of the device will increase [40], while for a thinner one, the Au NPs cannot be fully covered which leads to the exciton quenching by the Au NPs [15]. Thus their thicknesses are firstly optimized, and the thickness of MoO_3 layer is 2.5 nm for the reference device without Au NPs, while they are 4 nm for all the devices with Au layers.

Fig. 2(a) displays the J–V curves of the devices with different thickness of Au layers and their respectively optimized MoO_3 thickness. Each curve is averaged over four devices with the same configuration. The detailed photovoltaic parameters are summarized in Table 1. The reference device without Au layer shows a short-circuit current (Jsc), open-circuit voltage (Voc), fill factor (FF) of 5.53 mA/cm^2, 0.84 V, 0.64, corresponding to a PCE of 2.98%. The Voc of the devices increases from 0.84 to 0.86 V with the increase of Au layer thickness, which may be attributed to the increased built-in field due to Au has a higher work function than ITO. Meanwhile, the Jsc of the device increases significantly with the thickness of Au

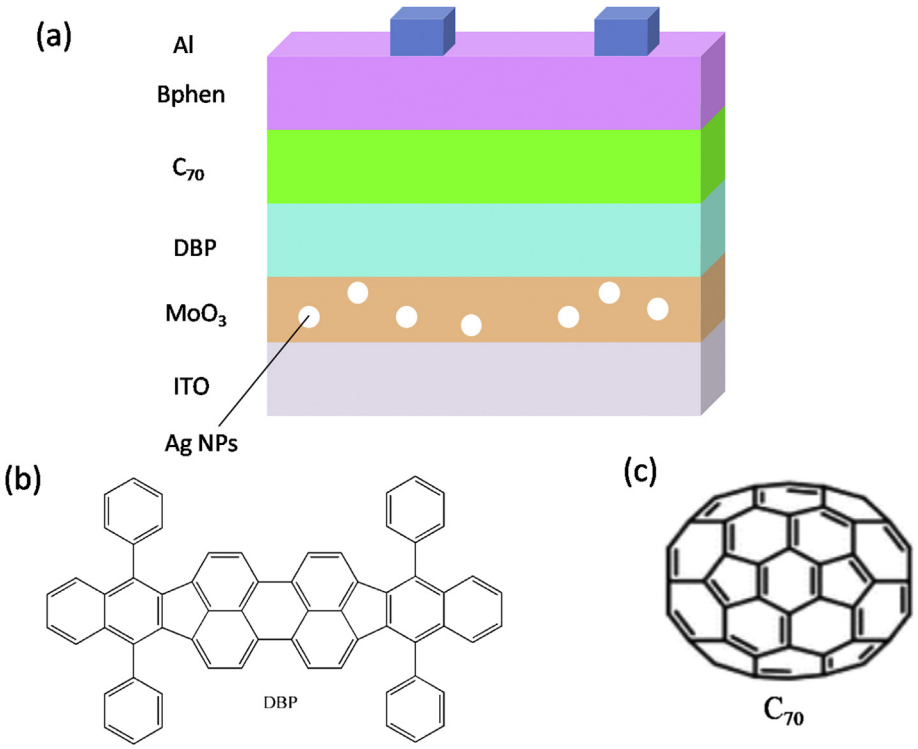

Fig. 1. (a) Device structure of the plasmonic OSCs, and the molecular chemical structures of (b) DBP and (c) C_{70}.

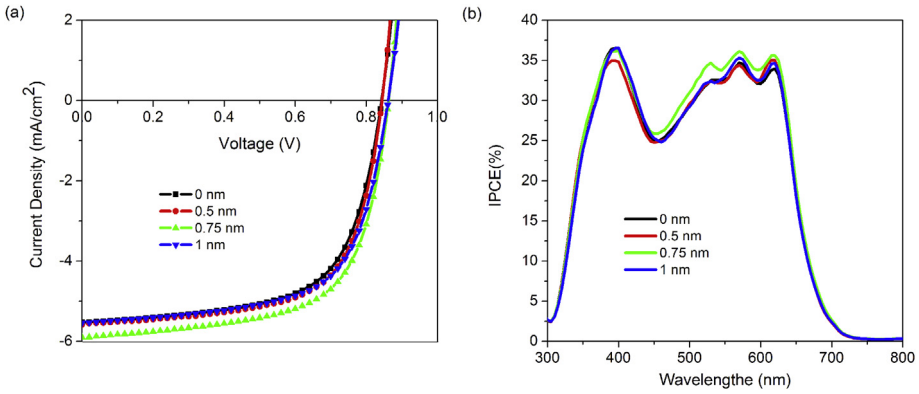

Fig. 2. (a) J-V curves and (b) IPCE spectra of the optimized devices with different thickness of Au layers.

Table 1
Photovoltaic parameters of the optimized devices with different thickness of Au layers.

Au thickness (nm)	MoO_3 thickness (nm)	Jsc (mA/cm^2)	Voc (V)	FF	PCE (%)	Jsc calculated from IPCE
0	2.5	5.53 ± 0.10	0.84 ± 0.01	0.64 ± 0.01	2.98 ± 0.02	5.44
0.5	4	5.58 ± 0.11	0.84 ± 0.01	0.63 ± 0.01	2.97 ± 0.06	5.42
0.75	4	5.89 ± 0.09	0.86 ± 0.01	0.65 ± 0.01	3.29 ± 0.06	5.69
1	4	5.54 ± 0.15	0.86 ± 0.01	0.64 ± 0.01	3.07 ± 0.09	5.46

layer, and the device with 0.75 nm Au layer exhibits the highest performance. This device shows a Jsc, Voc, FF, and PCE of 5.89 mA/cm^2, 0.86 V, 0.65, and 3.28%, respectively, and the champion device achieves a PCE of 3.40%. Compared with the reference device, the PCE is enhanced by more than 14%, and such an enhancement is primary attributed to the improvement of Jsc. This means the thermal evaporated Au layer indeed improves the performance of the OSCs. It should be noted that the Jsc of the device with 1 nm Au layer is decreased, which can be attributed to the increased probability of exciton quenching and lower intensity of light penetrated into the organic active layer due to the increased absorption and/or back scattering by the Au NPs with a higher density. Fig. 2(b) shows the IPCE spectra of the devices. All the devices present almost the same sharp of IPCE spectrum. The device with 0.75 nm Au layer has the highest IPCE in the whole visible region. The integrated Jsc values from the IPCE spectra of four devices are 5.44, 5.42, 5.69, and 5.46 mA/cm^2, respectively, which are listed in Table 1. The difference between integrated and measured Jsc are within 4%, indicating good accuracy of our J-V measurement.

To elucidate the origin of the improvement of Jsc, a series works

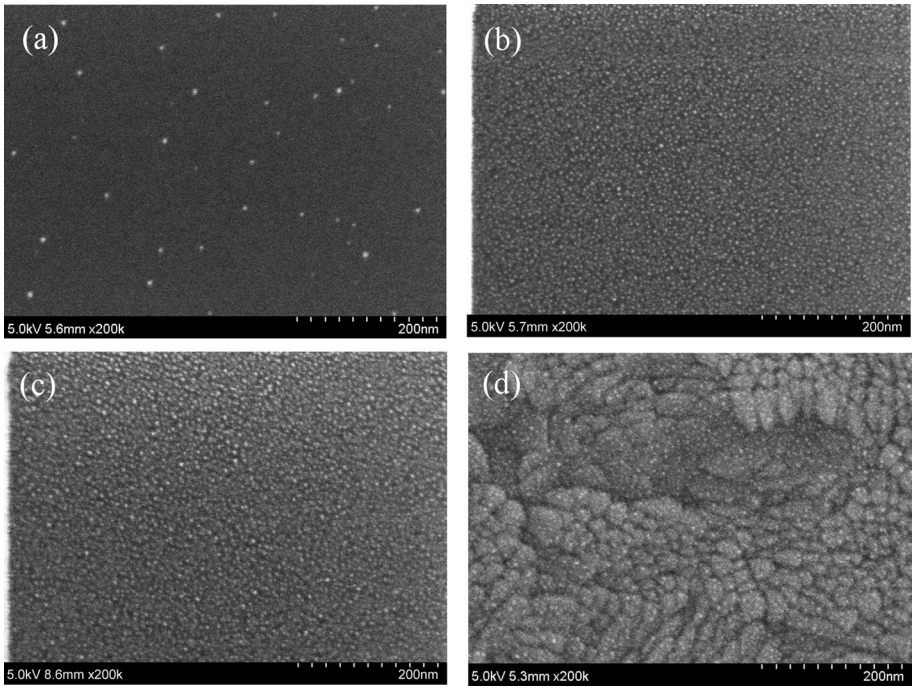

Fig. 3. SEM images of (a) 0.5, (b) 0.75, (c) 1 nm Au layers on Si wafers, and (d) 0.75 nm Au layer on an ITO glass substrate.

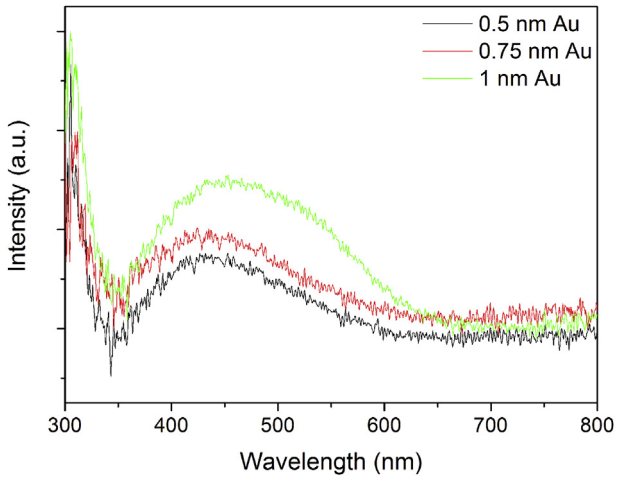

Fig. 4. Absorption spectra of Au layers with different thickness on ITO glass substrates.

are investigated. Fig. 3(a)–(c) show the SEM images of Au layers with different thickness on Si wafers. The thin Au layers used in this work are presented with the form of discontinued NPs. Because these Au NPs are small, smooth Si wafers are used to replace rough ITO as the testing substrates. We can find that the diameter of the Au NPs is about 5 nm, and the density of the NPs increases gradually with the thickness of Au layer. Fig. 3(d) shows the SEM image of 0.75 nm Au layer on an ITO glass substrate. Similar Au NPs are found as compared with that on Si wafer. This indicates that these two substrates have little effect on the morphology of the Au NPs.

The absorption spectra of different thickness Au films on the ITO-coated glass substrate are also measured, and the corresponding results are shown in Fig. 4. A characteristic peak at about 430 nm is existed for the 0.5 and 0.75 nm Au layers, while it shifts to 450 nm for 1 nm Au layer. Moreover, the absorption intensity increases with the thickness of Au layers. These absorptions can be assigned to the LSPR of Au NPs. The LSPR peak of metal NPs is determined by their particle size, shape, spacing, the dielectric properties, and dielectric environment [15,16]. Because the Au NPs in Au layers with different thickness have the same diameter, as shown in Fig. 3, both the red-shifted and increased absorption can be attributed to the increased Au NPs density.

In order to verify the effects of the LSPR of the Au NPs to the performance of the devices, we measure the absorption spectra of DBP (13 nm) on top of ITO/Au NPs/MoO_3 (the optimized thickness) with various thickness of Au layers. Because the absorption of Au NPs/MoO_3 can affect the total absorption efficiency of the films, we use Au NPs/MoO_3 films as the reference samples in the experiments to eliminate their contributions. So the absorption spectra represent only the light absorbance within DBP layers. All the DBP films on different Au layers exhibit an increased absorption as compared with that on bare MoO_3. A typical DBP absorption spectrum on 0.75 nm Au layer is shown in Fig. 5(a) to compare with that on bare MoO_3. An obvious enhancement is found over the range of 350–800 nm. This indicates that the LSPR of Au NPs can increase the absorption of organic layer deposited on them. LSPR of metal NPs can afford enhancement of the local electromagnetic field and scattering cross section, and both of these will increase the absorption efficiency. However, the diameter of Au NPs in this work is dramatically small than the incident light wavelength, thus the scattering effect can be ignored. This suggests the increase absorption is primary attributed to the enhancement of the local electromagnetic field.

To clearly demonstrate the effect of the enhanced absorption to Jsc, the difference between the absorptions (Δabs) as well as that of IPCE (ΔIPCE) before and after incorporating 0.75 nm Au layer are plotted simultaneously in Fig. 5(b). The two curves have the same sharp, which evinces that improved Jsc is attributed to the increased absorption of DBP. On the other hand, we can found that the absorption of DBP with Au NPs at 400–500 nm is almost twice as high as that of the reference one. However, the IPCE in this region only shows a slightly increase. As the electric field of the surface plasmon falls off evanescently perpendicular to the metal surface,

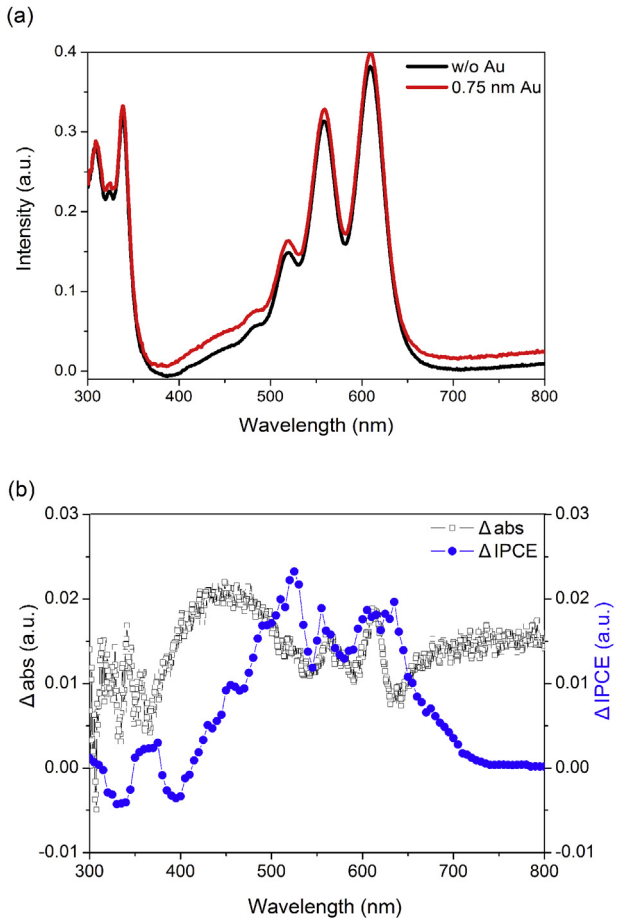

Fig. 5. (a) Absorption spectra of the ITO/(Au)/MoO_3(the optimized thickness)/DBP(60 nm) films without and with 0.75 nm Au layer, (b) Δabs of the films and ΔIPCE of the devices with and without Au NPs.

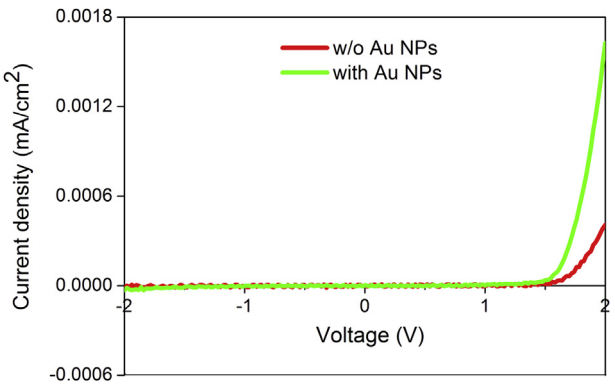

Fig. 6. J-V curves of the hole-only devices ITO/MoO_3/DBP/TAPC/Al with or without 0.75 nm Au.

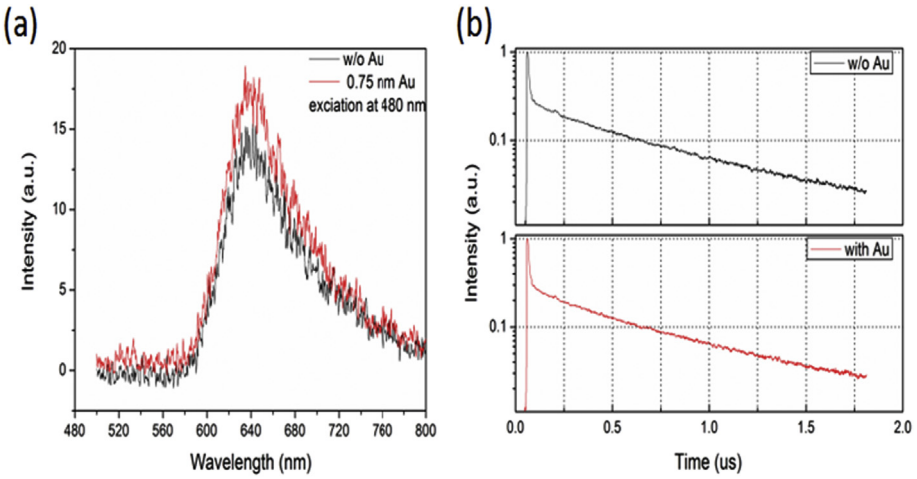

Fig. 7. (a) Steady-state PL spectra and (b) transient PL spectra of the MoO_3/DBP films with or without Au NPs.

the enhancement of DBP absorption will be more significantly in the region near the MoO_3/DBP interface. However, the photo-generated DBP excitons are dissociated at the DBP/C_{70} interface. This indicates that some of the DBP excitons generated in the region far from the DBP/C_{70} interface cannot be effectively dissociated.

Apart from the increased absorption, the incorporation of Au NPs may also result in the increase of conductivity [14,35,36] and the exciton dissociation probability due to the coupling between the excitons and LSPR [41]. To access these issues, hole only devices with the structure of ITO/Au (0 or 0.75 nm)/MoO_3 (the optimized thickness)/DBP (60 nm)/TAPC (1,1-bis-(4-bis(4-methyl-phenyl)-amino-phenyl)-cyclohexane) (20 nm)/Al (60 nm) have been fabricated. The dark currents of these devices are drawn in Fig. 6. It can be found that the current of the device with Au NPs is significant higher than that of reference device, especially in the positive voltage region. This indicates an increase of conductivity.

Fig. 7(a) shows the steady state PL spectra of Au (0 or 0.75 nm)/MoO_3 (the optimized thickness)/DBP (13 nm) films with an excitation at 480 nm. The excitation wavelength was selected intentionally to be located within the LSPR region of Au NPs (see Fig. 4). The two films appear a similar PL spectrum with the peak at 650 nm, which can be assigned to the emission of DBP. On contrast, the PL intensity of the film with Au NPs is enhanced by ca. 25%. We attribute the enhanced PL intensity to the fact that the LSPR of Au NPs increases the degree of light absorption and thereby, enhances the light excitation rate. This can be attributed to the resonance frequency of the Au NPs closed to the absorption band of DBP. This phenomenon is consistent with our measured device characteristics, as depicted in Fig. 2. Fig. 7(b) shows the undeconvoluted transient decay curves of the MoO_3/DBP films with or without 0.75 nm Au layer. The excitation wavelength is 480 nm, which matches the LSPR of Au NPs. The transient decays of the DBP films with or without Au NPs have the same profile. This means any modifications of the excitonic states of the DBP film that resulted from the coupling between the excitons and the LSPR can be neglected when a 4 nm MoO_3 buffer layer is used. Therefore, the results further confirm that the increased DBP PL intensity can be attributed to the increased light absorption and exciton generation upon excitation of the LSPR.

4. Conclusion

In summary, high efficient surface plasmon enhanced all thermal evaporated small molecule OSCs are demonstrated by incorporation Au NPs. The optimized device with a 0.75 nm Au layer shows a peak PCE of 3.40%, which is 14.1% higher than the reference device without Au NPs. The enhanced PCE is primary result from the improved Jsc, which is attributed to the increased absorption due to the near-field enhancement of the LSPR of Au NPs and the conductivity of the devices. The method we report herein is simple and cost-effective, which provides a route for developing high performance all thermal evaporated OSCs by utilizing plasmonic effect.

Acknowledgements

This work was supported by the National Natural Science Foundation of China (11004187, 61575192, 61376062, and 61376022) and the Science and Technology Development Plan of Jilin Province (20140201094JC).

References

[1] A.R.B.M. Yusoff, D. Kim, H.P. Kim, F.K. Shneider, W.J. da Silva, J. Jang, A high efficiency solution processed polymer inverted triple-junction solar cell exhibiting a power conversion efficiency of 11.83%, Energy Environ. Sci. 8 (2015) 303–316.
[2] Z. He, B. Xiao, F. Liu, H. Wu, Y. Yang, S. Xiao, C. Wang, T.P. Russell, Y. Cao, Single-junction polymer solar cells with high efficiency and photovoltage, Nat. Photonics 9 (2015) 174–179.
[3] X. Ouyang, R. Peng, L. Ai, X. Zhang, Z. Ge, Efficient polymer solar cells employing a non-conjugated small-molecule electrolyte, Nat. Photonics 9 (2015) 520–524.
[4] Y. Liu, C.C. Chen, Z. Hong, J. Gao, Y.M. Yang, H. Zhou, L. Dou, G. Li, Y. Yang, Solution-processed small-molecule solar cells: breaking the 10% power conversion efficiency, Sci. Rep. 3 (2013) 3356.
[5] J. You, C.C. Chen, Z. Hong, K. Yoshimura, K. Ohya, R. Xu, S. Ye, J. Gao, G. Li, Y. Yang, 10.2% power conversion efficiency polymer tandem solar cells consisting of two identical sub-cells, Adv. Mater 25 (2013) 3973–3978.
[6] S. Liu, P. You, J. Li, J. Li, C.-S. Lee, B.S. Ong, C. Surya, F. Yan, Enhanced efficiency of polymer solar cells by adding a high-mobility conjugated polymer, Energy Environ. Sci. 8 (2015) 1463–1470.
[7] V. Vohra, K. Kawashima, T. Kakara, T. Koganezawa, I. Osaka, K. Takimiya, H. Murata, Efficient inverted polymer solar cells employing favourable molecular orientation, Nat. Photonics 9 (2015) 403–408.
[8] N. Li, C.J. Brabec, Air-processed polymer tandem solar cells with power conversion efficiency exceeding 10%, Energy Environ. Sci. 8 (2015) 2902–2909.
[9] W. Yu, L. Huang, D. Yang, P. Fu, L. Zhou, J. Zhang, C. Li, Efficiency exceeding 10% for inverted polymer solar cells with a ZnO/ionic liquid combined cathode interfacial layer, J. Mater. Chem. A 3 (2015) 10660–10665.
[10] J. You, L. Dou, K. Yoshimura, T. Kato, K. Ohya, T. Moriarty, K. Emery, C.C. Chen, J. Gao, G. Li, Y. Yang, A polymer tandem solar cell with 10.6% power conversion efficiency, Nat. Commun. 4 (2013) 1446.
[11] L. Liu, W.E. Stanchina, G. Li, Effects of semiconducting and metallic single-walled carbon nanotubes on performance of bulk heterojunction organic solar cells, Appl. Phys. Lett. 94 (2009) 233309.

[12] Y. Jin, J. Feng, X.-L. Zhang, M. Xu, Y.-G. Bi, Q.-D. Chen, H.-Y. Wang, H.-B. Sun, Surface-plasmon enhanced absorption in organic solar cells by employing a periodically corrugated metallic electrode, Appl. Phys. Lett. 101 (2012) 163303.
[13] C.J. Brabec, N.S. Sariciftci, J.C. Hummelen, Plastic solar cells, Adv. Funct. Mater 11 (2001) 15–26.
[14] M. Xu, J. Feng, Y.-S. Liu, Y. Jin, H.-Y. Wang, H.-B. Sun, Effective and tunable light trapping in bulk heterojunction organic solar cells by employing Au-Ag alloy nanoparticles, Appl. Phys. Lett. 105 (2014) 153303.
[15] Z. Su, L. Wang, Y. Li, G. Zhang, H. Zhao, H. Yang, Y. Ma, B. Chu, W. Li, Surface plasmon enhanced organic solar cells with a MoO_3 buffer layer, ACS Appl. Mater. Interfaces 5 (2013) 12847–12853.
[16] F. Jin, B. Chu, W. Li, Z. Su, H. Zhao, C.S. Lee, Enhanced performances in inverted small molecule solar cells by Ag nanoparticles, Opt. Express 22 (2014) A1669.
[17] E. Hutter, J.H. Fendler, Exploitation of localized surface plasmon resonance, adv, Mater 16 (2004) 1685–1706.
[18] X. Chen, B. Jia, Y. Zhang, M. Gu, Exceeding the limit of plasmonic light trapping in textured screen-printed solar cells using Al nanoparticles and wrinkle-like graphene sheets, Light Sci. Appl. 2 (2013) e92.
[19] Y. Jin, J. Feng, M. Xu, X.-L. Zhang, L. Wang, Q.-D. Chen, H.-Y. Wang, H.-B. Sun, Matching photocurrents of sub-cells in double-junction organic solar cells via coupling between surface plasmon polaritons and microcavity modes, Adv. Opt. Mater 1 (2013) 809–813.
[20] V. Janković, Y. Yang, J. You, L. Dou, Y. Liu, P. Cheung, J.P. Chang, Y. Yang, Active layer-incorporated, spectrally tuned Au/SiO2 core/shell nanorod-based light trapping for organic photovoltaics, ACS Nano 7 (2013) 3815–3822.
[21] Y.-S. Hsiao, S. Charan, F.-Y. Wu, F.-C. Chien, C.-W. Chu, P. Chen, F.-C. Chen, Improving the light trapping efficiency of plasmonic polymer solar cells through photon management, J. Phys. Chem. C 116 (2012) 20731–20737.
[22] C.H. Chou, F.C. Chen, Plasmonic nanostructures for light trapping in organic photovoltaic devices, Nanoscale 6 (2014) 8444–8458.
[23] V. Kumar, H. Wang, Plasmonic Au nanoparticles for enhanced broadband light absorption in inverted organic photovoltaic devices by plasma assisted physical vapour deposition, Org. Electron 14 (2013) 560–568.
[24] G.-Q. Fan, Q.-Q. Zhuo, J.-J. Zhu, Z.-Q. Xu, P.-P. Cheng, Y.-Q. Li, X.-H. Sun, S.-T. Lee, J.-X. Tang, Plasmonic-enhanced polymer solar cells incorporating solution-processable Au nanoparticle-adhered graphene oxide, J. Mater. Chem. 22 (2012) 15614.
[25] Y. Xiao, J.P. Yang, P.P. Cheng, J.J. Zhu, Z.Q. Xu, Y.H. Deng, S.T. Lee, Y.Q. Li, J.X. Tang, Surface plasmon-enhanced electroluminescence in organic light-emitting diodes incorporating Au nanoparticles, Appl. Phys. Lett. 100 (2012) 013308.
[26] W.C. Choy, The emerging multiple metal nanostructures for enhancing the light trapping of thin film organic photovoltaic cells, Chem. Commun. 50 (2014) 11984–11993.
[27] X. Ren, J. Cheng, S. Zhang, X. Li, T. Rao, L. Huo, J. Hou, W.C. Choy, High efficiency organic solar cells achieved by the simultaneous plasmon-optical and plasmon-electrical effects from plasmonic asymmetric modes of gold nanostars, Small (2016), http://dx.doi.org/10.1002/smll.201601949.
[28] X. Chen, X. Yang, W. Fu, M. Xu, H. Chen, Enhanced performance of polymer solar cells with a monolayer of assembled gold nanoparticle films fabricated by Langmuir–Blodgett technique, Mater. Sci. Eng. B 178 (2013) 53–59.
[29] X. Chen, L. Zuo, W. Fu, Q. Yan, C. Fan, H. Chen, Insight into the efficiency enhancement of polymer solar cells by incorporating gold nanoparticles, Sol. Energy Mater. Sol. Cells 111 (2013) 1–8.
[30] W. Wang, Y. Hao, Y. Cui, X. Tian, Y. Zhang, H. Wang, F. Shi, B. Wei, W. Huang, High-efficiency, broad-band and wide-angle optical absorption in ultra-thin organic photovoltaic devices, Opt. Express 22 (Suppl 2) (2014) A376–A385.
[31] L. Lu, Z. Luo, T. Xu, L. Yu, Cooperative plasmonic effect of Ag and Au nanoparticles on enhancing performance of polymer solar cells, Nano Lett. 13 (2013) 59–64.
[32] J.-L. Wu, F.-C. Chen, Y.-S. Hsiao, F.-C. Chien, P. Chen, C.-H. Kuo, M.H. Huang, C.-S. Hsu, Surface plasmonic effects of metallic nanoparticles on the performance of polymer bulk heterojunction solar cells, ACS Nano 5 (2011) 959–967.
[33] E. Stratakis, E. Kymakis, Nanoparticle-based plasmonic organic photovoltaic devices, Mater. Today 16 (2013) 133–146.
[34] F.-X. Xie, W.C.H. Choy, C.C.D. Wang, W.E.I. Sha, D.D.S. Fung, Improving the efficiency of polymer solar cells by incorporating gold nanoparticles into all polymer layers, Appl. Phys. Lett. 99 (2011) 153304.
[35] H.L. Gao, X.W. Zhang, Z.G. Yin, H.R. Tan, S.G. Zhang, J.H. Meng, X. Liu, Plasmon enhanced polymer solar cells by spin-coating Au nanoparticles on indium-tin-oxide substrate, Appl. Phys. Lett. 101 (2012) 133903.
[36] C.-S. Kao, F.-C. Chen, C.-W. Liao, M.H. Huang, C.-S. Hsu, Plasmonic-enhanced performance for polymer solar cells prepared with inverted structures, Appl. Phys. Lett. 101 (2012) 193902.
[37] D. Gaspar, A.C. Pimentel, T. Mateus, J.P. Leitao, J. Soares, B.P. Falcao, A. Araujo, A. Vicente, S.A. Filonovich, H. Aguas, R. Martins, I. Ferreira, Influence of the layer thickness in plasmonic gold nanoparticles produced by thermal evaporation, Sci. Rep. 3 (2013) 1469.
[38] X. Chen, C. Zhao, L. Rothberg, M.-K. Ng, Plasmon enhancement of bulk heterojunction organic photovoltaic devices by electrode modification, Appl. Phys. Lett. 93 (2008) 123302.
[39] M.J. Beliatis, S.J. Henley, S. Han, K. Gandhi, A.A. Adikaari, E. Stratakis, E. Kymakis, S.R. Silva, Organic solar cells with plasmonic layers formed by laser nanofabrication, Phys. Chem. Chem. Phys. 15 (2013) 8237–8244.
[40] V. Shrotriya, G. Li, Y. Yao, C.W. Chu, Y. Yang, Transition metal oxides as the buffer layer for polymer photovoltaic cells, Appl. Phys. Lett. 88 (2006) 073508.
[41] D.D.S. Fung, L. Qiao, W.C.H. Choy, C. Wang, W.E.I. Sha, F. Xie, S. He, Optical and electrical properties of efficiency enhanced polymer solar cells with Au nanoparticles in a PEDOT-PSS layer, J. Mater. Chem. 21 (2011) 16349–16356.